



Published in final edited form as:

Proc SPIE Int Soc Opt Eng. 2013 March 13; 8669: 866907-. doi:10.1117/12.2006977.

Fiber feature map based landmark initialization for highly deformable DTI registration

Aditya Gupta^{a,c}, Matthew Toews^b, Ravikiran Janardhana^d, Yogesh Rathi^b, John Gilmore^c, Maria Escolar^a, and Martin Styner^{c,d}

^aDept Pediatrics, University of Pittsburgh, PA, USA

^bHarvard Medical School, Boston MA

^cDept Psychiatry, University of North Carolina, Chapel Hill, NC

^dDept Computer Science, University of North Carolina, Chapel Hill, NC

Abstract

This paper presents a novel pipeline for the registration of diffusion tensor images (DTI) with large pathological variations to normal controls based on the use of a novel feature map derived from white matter (WM) fiber tracts. The research presented aims towards an atlas based DTI analysis of subjects with considerable brain pathologies such as tumors or hydrocephalus. In this paper, we propose a novel feature map that is robust against variations in WM fiber tract integrity and use these feature maps to determine a landmark correspondence using a 3D point correspondence algorithm. This correspondence drives a deformation field computed using Gaussian radial basis functions(RBF). This field is employed as an initialization to a standard deformable registration method like demons. We present early preliminary results on the registration of a normal control dataset to a dataset with abnormally enlarged lateral ventricles affected by fatal demyelinating Krabbe disease. The results are analyzed based on a regional tensor matching criterion and a visual assessment of overlap of major WM fiber tracts. While further evaluation and improvements are necessary, the results presented in this paper highlight the potential of our method in handling registration of subjects with severe WM pathology.

Keywords

fiber feature map; 3D point correspondence; DTI; large deformation fields

1. INTRODUCTION

Diffusion tensor imaging (DTI) has proven especially of value in clinical studies of white matter (WM) integrity in the developing brain. In this paper, we focus on the application of DTI in a natural history study of a particularly devastating WM demyelinating disease called Krabbe.¹ Previous studies show that neonates with infantile Krabbe disease have lower fractional anisotropy (FA) across the corpus callosum and along the DTI fiber bundle of

internal capsules (IC) when compared with healthy age-matched controls.² Based on the above findings, atlas based fiber tract analysis is used for analyzing DTI of Krabbe subjects.³ For accurate analysis of WM fiber tracts it is crucial to establish a registration based voxel-wise correspondence between a normal control and the Krabbe subjects.

In addition to the pathological WM integrity, untreated infantile Krabbe cases may develop significantly enlarged lateral ventricles, a condition similar to hydrocephalus. The enlargement of the lateral ventricles push the fiber tracts against the skull, making it very difficult to analyze these images with an atlas based methodology. In our studies, the clinicians are interested to investigate fiber tracts based DTI analysis in such natural history cases as this reveals crucial information about disease progression.

The research in this paper is a step towards the analysis of these fiber tracts. The paper presents a method to determine point correspondences between the subject case and the normal control automatically by computing novel feature maps from the DWI data. These feature maps highlight the crossing fiber regions and are based on voxel-wise fiber density and entropy computations. The point correspondences are used to determine a deformation field via Gaussian radial basis functions (RBF).⁴ This deformation field is then used to initialize a standard registration method. The results are presented on a Krabbe subject with particularly abnormal enlarged ventricles to highlight the potential of the proposed approach.

The main contributions of this paper include a novel feature map determined from DWI data, which highlights the single and crossing fiber geometry, while being robust against variations in WM fiber tract integrity, a feature desirable in many WM demyelinating pathologies. Also this paper proposes a novel registration pipeline, which uses this feature map alongside a 3D correspondence algorithm and a Gaussian RBF to initialize standard registration algorithms to handle high anatomical deformations.

2. METHODOLOGICAL BACKGROUND

Registration of DTIs is particularly challenging, as DTI data is multi-dimensional and the tensor orientations after image transformations must remain consistent with the anatomy. Prior to the development of full tensor based registration methods, DTI registration was performed with traditional image registration algorithms on scalar images derived from the DTI. The performance of scalar and full tensor registration algorithms are compared for Krabbe neonates⁵ and the full tensor based DTI-TK⁶ method showed the most accurate performance.

The major drawback when using DTI derived FA scalar map in the registration of WM demyelinating pathologies is that the FA values are majorly affected by the pathology. While intensity normalization approaches have been employed to reduce the impact of this issue, major pathologies cannot be handled in this way. This drives the motivation of our proposed work towards a feature map that is robust against variations in WM fiber tract integrity. Several authors have used other DTI derived scalar maps such as radial diffusivity (RD), mean diffusivity (MD) or even multichannel registration⁷ with several of these feature

maps. But again these methods rely on properties derived from the fiber tracts, which may be an issue in pathologies such as Krabbe with large structural variations. The motivation of our proposed feature map is to highlight voxel-wise fiber geometry features such as crossing fiber and single fiber situations, which can be largely independent of the fiber tract properties and thus be used as the driving force for registration. The next section discusses the methodology behind generating these feature maps, the point correspondence, initial deformation field and the final deformation.

3. METHODS

The first part of this section describes the steps involved in generating the novel feature map from DWI data. The second part describes the algorithm for determining the point correspondence on these feature maps. This is followed by a description on using the point correspondences to determine an initial deformation field through Gaussian RBF. Finally the steps involved in using this deformation field as an initialization to a standard registration algorithm are discussed.

3.1 Feature Map Generation

To generate the feature map, we first perform whole brain, two-tensor unscented kalman filter based tractography directly from the DWI images to obtain the fiber tracts image. From the resulting dense set of fiber tracts, we compute two sets of features namely, 1) the proportion of fiber tracts passing through each voxel and 2) the entropy of fiber orientations for each voxel. We normalize and combine these two features in order to develop a single feature image.

Fiber Tracts Generation—The fiber tracts are generated from the raw DWI image and a full brain image mask by performing a two-tensor unscented kalman filter based tractography. The in-depth details of the two tensor tractography have been described previously in literature.⁸ While generating the fiber tracts for our experiments, we configured the number of seeds per voxel as 8, seed FA limit as 0.18, minimum FA to continue tractography as 0.12 and branching was suppressed while using multiple tensors. Unlike many of the existing techniques, in ukf-based tractography, fiber tracking is formulated as causal estimation; at each step of tracing the fiber, the current estimate of the signal is guided by the previous. To do this, the signal is modeled as a discrete mixture of Watson directional functions and tractography is performed within a filtering framework. Starting from a seed point, each fiber is traced to its termination using an unscented Kalman filter to simultaneously fit the signal and propagate in the most consistent direction. Despite the presence of noise and uncertainty, this provides an accurate estimate of the local structure at each point along the fiber.

Fiber Segments per voxel—In this step, we traverse through all the fiber segments of the generated fiber tracts. A normalized image is then computed that shows the voxel-wise proportion of fibers segments in a given voxel.

Entropy of Fiber Orientations—For this map, we compute the entropy of fiber orientations in all fiber segments that pass through at a particular voxel. The fiber

orientations are determined as the direction of the tangent joining its neighboring fiber segment points (figure 1). At the start and end fiber points, the fiber orientation is defined as the direction of the line connecting it to the previous or subsequent fiber point. This histogram of fiber orientations per voxel is computed on a unit sphere that is subdivided into uniform regions standard icosahedron spherical subdivision. Given a fiber orientation, we first find its enclosing icosahedron triangular face on the unit sphere and add relative contributions to the triangles three vertices using barycentric coordinates. This spherical histogram is then used to generate the entropy of fiber orientations. For a single-fiber voxel we expect lower entropy, whereas for multiple fiber tracts and multiple fiber orientations, we expect comparatively higher entropy. Using the histogram, we compute entropy of fiber orientations per voxel as below:

$$H(X) = - \sum_{i=1}^n p(x_i) \log_b p(x_i) \quad (1)$$

where, $H(X)$ is the entropy of fiber orientation at a particular voxel, $p(x_i)$ is the probability of a fiber orientation the voxel x_i and n represents all possible fiber orientations.

Features combination—We obtain the final feature map quite straightforwardly by computing the product of the normalized values of the two features.

$$F_i(X) = \frac{H_i(X)}{\max H(X)} * \frac{fs_i(X)}{\max fs(X)} \quad (2)$$

where $F_i(X)$, $H_i(X)$ and $fs_i(X)$ are the feature map value, entropy of fiber orientations and the number of fiber segments at voxel i respectively, $\max H(X)$ and $\max fs(X)$ are the maximum values of entropy of fiber orientations and number of fiber segments over the entire image.

3.2 Landmarks with correspondence on feature maps

Deformable intensity-based image registration methods employ local optimization methods that largely driven by distinctive image structure, i.e. corners or landmarks, and must be correctly initialized in order ensure convergence to correct solutions. Here, we achieve initialization from a set of robust image-to-image correspondences obtained via a 3D version of the scale-invariant feature transform (SIFT) matching technique of Lowe et al.⁹ The SIFT technique operates by identifying maxima in a difference-of-Gaussian (DoG) operator:

$$\{x, y, z, \sigma\} = \text{local argmax}_{x, y, z, \sigma} \{|G(x, y, z, \sigma) - G(x, y, z, \kappa\sigma)|\}, \quad (3)$$

where $G(x, y, z, \sigma)$ represents the convolution with a Gaussian operator of variance σ^2 and κ is a constant. Image regions centered on x, y, z of size proportional to σ are then cropped and spatially normalized via rescaling and reorientation to a local coordinate system,¹⁰ and encoded as an appearance descriptor. Image-to-image matching proceeds by computing nearest neighbors between features extracted in different images, based on the Euclidean distances of appearance descriptors. Note that due to spatial feature normalization, nearest neighbors can be computed despite arbitrary global similarity image transforms (i.e. translation, rotation and isotropic scaling). Finally, the Hough transform is applied to

determine a set of correspondences that are inliers of a robust image-to-image similarity transform.

3.3 Registration

Due to the large variation between the normal control and the subject with enlarged ventricles, a large deformation field is needed to register these images. Registration failed with the standard registration algorithms, including B-spline based (fnirt in FSL package), fluid based (fWarp in FSL), Demons (BRAINSDemonWarp in BRAINS) and also full tensor registration method DTITK within the DTI-Toolkit package. All the above methods failed to provide the large deformation required to register these images, particularly in the regions around the enlarged ventricles (figure 4).

To determine the large local deformation field, we first use the landmark correspondences to compute an initial deformation field. The computed landmarks are in general well distributed over the image and hence have the capability to estimate a global deformation field from these local landmarks. We use Gaussian radial basis functions (RBF) to determine the initial deformation field as implemented in the plastimatch registration toolkit. A Gaussian RBF decreases with growing distance from the landmark and the RBF asymptotically approaches zero. These properties along with the option of not selecting a polynomial part for RBF, give the desired advantage of decreasing global influence with higher distance from the landmarks. While we selected a straightforward landmark based deformation field generation in this work, there is lot of ongoing research in generating deformation fields from landmark points that potentially can improve the performance of our proposed registration approach. Once the deformation field is obtained, this field is used to initialize a deformable registration like diffeomorphic demons registration on intensity normalized FA images. The results of the combined fields - the point landmark deformation field and the demons deformation field on the FA images are presented in the next section.

4. RESULTS

To prove the potential of our method, we select a particular subject with abnormally large lateral ventricles. Figure 4 (a and d) shows the FA images of the Krabbe case and the normal control. A visual analysis of the large difference in the structure of the moving and the target images indicates the challenging problem at hand. The Krabbe case shows how due to the enlargement of the lateral ventricle the fiber tracts are pushed towards the cortical surface. Also it is interesting to note that the fiber tracts like the internal capsules, genu and splenium change their shape to take the shape of the enlarged lateral ventricle. Below we present the results of the various steps in our method and a visual and quantitative evaluation of our registration method.

The feature maps generated from the DWI volumes of the subject and the normal control, as described in 3.1, are shown in figure 2. The figure shows the image representing the fiber segments per voxel, the normalized entropy and the combined final map. For the image representing the fiber segments per voxel, high intensity regions are expected and observed in regions of single fiber tracts and crossing fibers, as both capture a large proportion of fiber segments. For the entropy image, the high intensities are regions of dispersed fiber

tracts (e.g., close to gray matter) and crossing fiber tracts (due to greater variation in fiber orientations) and the lower intensities are regions of unidirectional single fiber tracts (or regions with lack of fiber tracts). The combination of these two features results in comparatively lower intensities for the unidirectional single fiber situation as compared to crossing fiber situations. Furthermore, locations close or in gray matter display very low intensities in the combined map. In comparison, FA maps cannot successfully highlight crossing fiber locations as these have often similar intensities as WM regions.

The combined feature map images for the subject and the normal control are then used as input to determine the point landmark correspondence. Since the feature maps have high intensity for the crossing fibers, this helps the point correspondence algorithm to determine good correspondences in spite of the large deformation. Figure 3 shows an example of one set of correspondence landmark points determined by this algorithm. Particularly in pathological cases where it is extremely difficult to even manually determine the landmarks because of the large abnormal deformation, our proposed method gives a considerable advantage.

The point correspondences are used as inputs to the Gaussian RBF to determine the initial deformation field. The deformation field obtained from the point correspondence provides the required initialization for standard registration algorithms. This deformation field is used to initialize the demons algorithm applied on the subject and the normal control FA images. Figure 4 shows the registration results using Demons (4b), DTITK (4c) and our proposed method (4e and 4f). Clearly Demons and DTITK fail to produce the required deformation to push the corticospinal and the internal capsule tracts towards the necessary locations in the pathological subject. Also the figure (4f) shows the overlap of the target and the image registered with our method for a visual evaluation of the registration performance. The regions in orange indicate the WM fiber tracts that are aligned successfully. The orange color for the fiber tracts indicates a considerable success in registration for the major tracts - the genu, splenium and the internal capsule tracts compared to the other standard registration methods.

To further evaluate the registration, we use average regional matching criterion that is tailored to atlas based analysis methods. The orientation agreement between the principal eigenvectors of the source e_{source} and the target e_{target} weighted with the FA value of the target of each voxel of a particular region is the basis of this criterion. Regions of interest (ROI) on the Krabbe subject are defined representing major fiber tracts. For a ROI r , the average regional matching criterion is defined as:

$$RegMatch_r = \frac{1}{N_r} \sum_{i=1}^{N_r} |e_{source} \cdot e_{target}| \cdot FA_{target} \cdot N_r \quad (4)$$

representing number of voxels in region r . The RegMatch percent values for the comparison of Demons, DTITK and our proposed method for three ROIs (100% indicates perfect registration) are shown in Figure 5. Considering the three ROIs, our proposed shows an improvement of 15.4% over DTITK and 22.8% over Demons method.

5. DISCUSSIONS AND CONCLUSIONS

In this paper, we have presented a novel, fully automatic pipeline to register images with large deformations, particularly subjects that are affected by WM demyelinating pathologies. The novel feature map computed is robust against variations in WM fiber tract integrity and hence yields a good starting point to compute corresponding landmark points. The work presented here shows the potential of our pipeline to register highly deformed images as illustrated on a single, highly pathological case. We have applied the method to several more Krabbe cases with moderate to severely enlarged ventricles with similar success. Nevertheless, the presented registration pipeline is preliminary and several issues still need to be addressed, such as improving the stability of the landmark based deformation field computation against outliers/bad correspondences. For that purpose, we are currently working on incorporating weights for each landmark based on their correspondence quality score.

REFERENCES

1. Escolar M, Poe M, Smith J, Gilmore J, Kurtzberg J, Lin W, Styner M. Diffusion tensor imaging detects abnormalities in the corticospinal tracts of neonates with infantile krabbe disease. *American Journal of Neuroradiology*. 2009 May; 30(5):1017–1021. [PubMed: 19386732]
2. Guo AC, Petrella JR, Kurtzberg J, Provenzale JM. Evaluation of white matter anisotropy in krabbe disease with diffusion tensor mr imaging: Initial experience1. *Radiology*. 2001; 218(3):809–815. [PubMed: 11230660]
3. Goodlett C, Davis B, Jean R, Gilmore J, Gerig G. Improved correspondence for dti population studies via unbiased atlas building. 2006; 9:260–267.
4. Fornefett M, Rohr K, Stiehl HS. Elastic registration of medical images using radial basis functions with compact support. *Proc. Computer Vision and Pattern Recognition*. 1999:402407.
5. Wang Y, Gupta A, Liu Z, Zhang H, Escolar ML, Gilmore JH, Gouttard S, Fillard P, Maltbie E, Gerig G, Styner M. Dti registration in atlas based fiber analysis of infantile krabbe disease. *NeuroImage*. 2011; 55(4):1577–1586. [PubMed: 21256236]
6. Zhang H, Yushkevich PA, Alexander DC, Gee JC. Deformable registration of diffusion tensor mr images with explicit orientation optimization. *Medical Image Analysis*. 2006; 10(5):764–785. [PubMed: 16899392]
7. Alexander DC, Gee JC, Bajcsy R. Similarity measures for matching diffusion tensor images. *British Machine Vision Conference*. 1999
8. Malcolm JG, Michailovich O, Bouix S, Westin C-F, Shenton ME, Rathi Y. A ltered approach to neural tractography using the watson directional function. *Medical Image Analysis*. 2010:58–69. [PubMed: 19914856]
9. Lowe DG. Distinctive image features from scale-invariant keypoints. *IJCV*. 2004; 60(2):91–110.
10. Allaire, S.; Kim, J.; Breen, S.; Jaffray, D.; Pekar, V. [MMBIA]. 2008. Full orientation invariance and improved feature selectivity of 3d sift with application to medical image analysis.

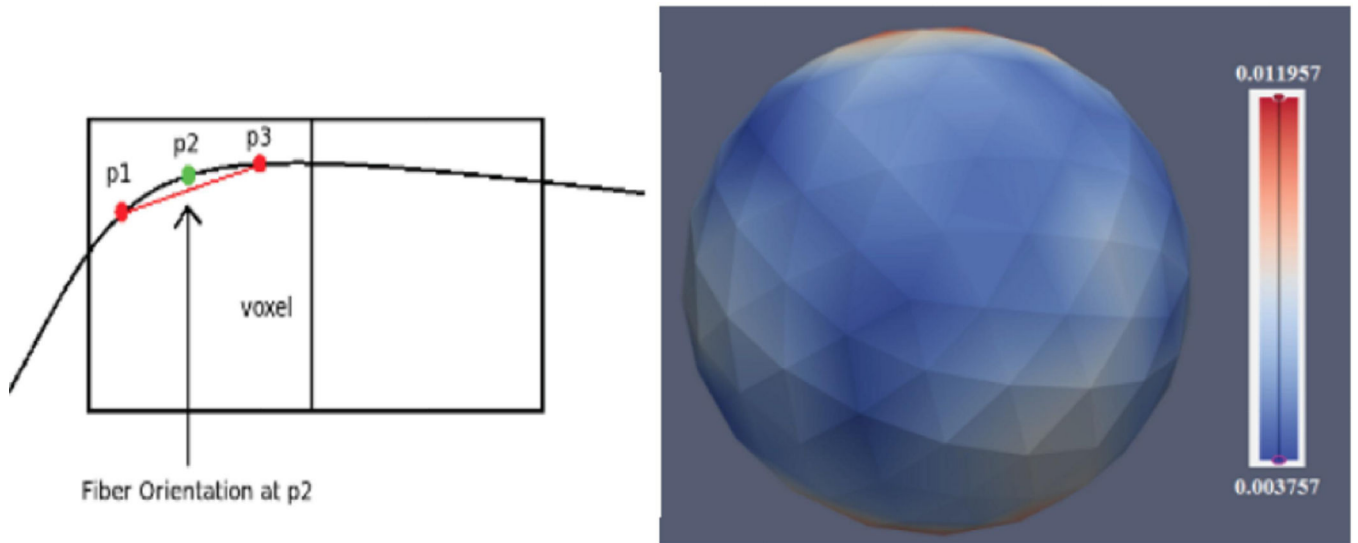


Figure 1. Fiber orientation computed at a fiber segment point and the histogram representing the fiber orientations of a particular voxel on a unit sphere.

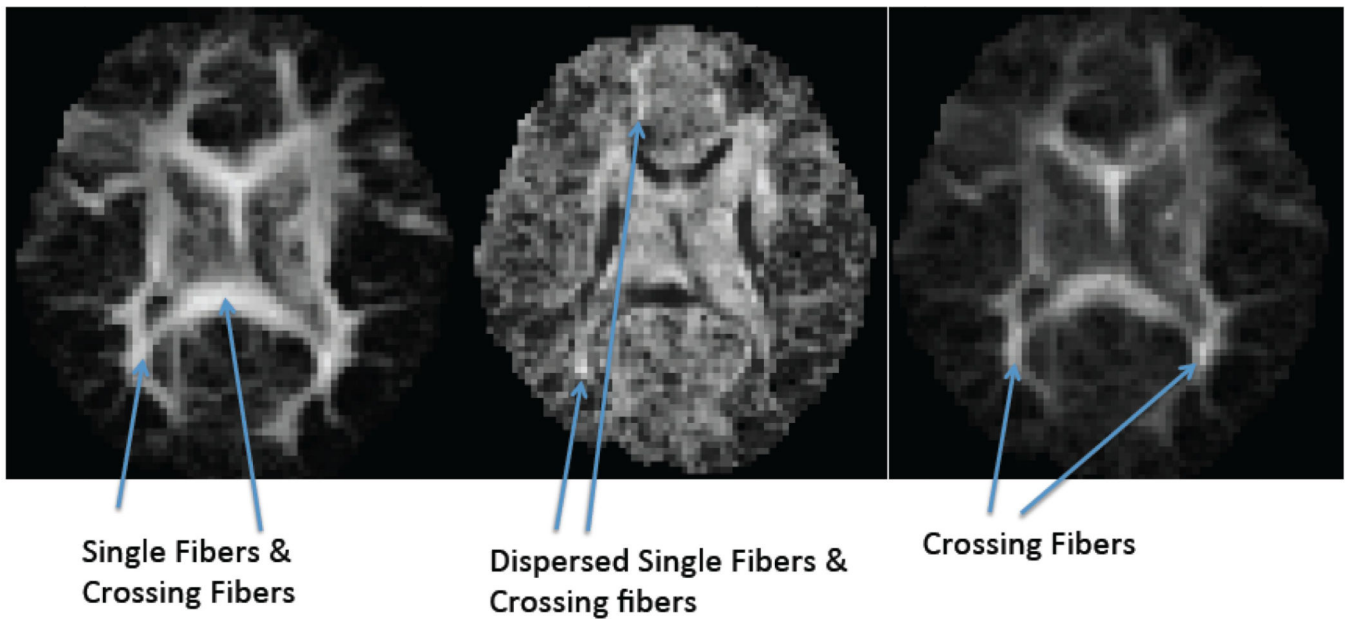


Figure 2.
Feature maps in normal control subject. Left: Fiber Segments per voxel image;
Center: Entropy of fiber orientations per voxel image; Right: the combined feature map
image. The regions with crossing fibers are marked with arrows and display a high intensity
in the final feature map.

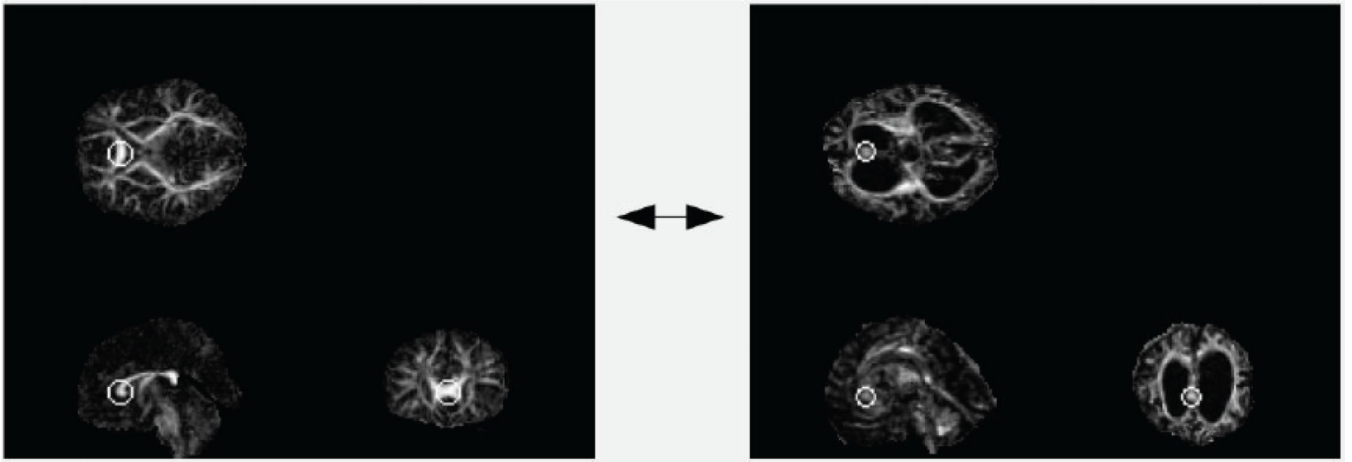


Figure 3.
Example of one set of correspondence points.

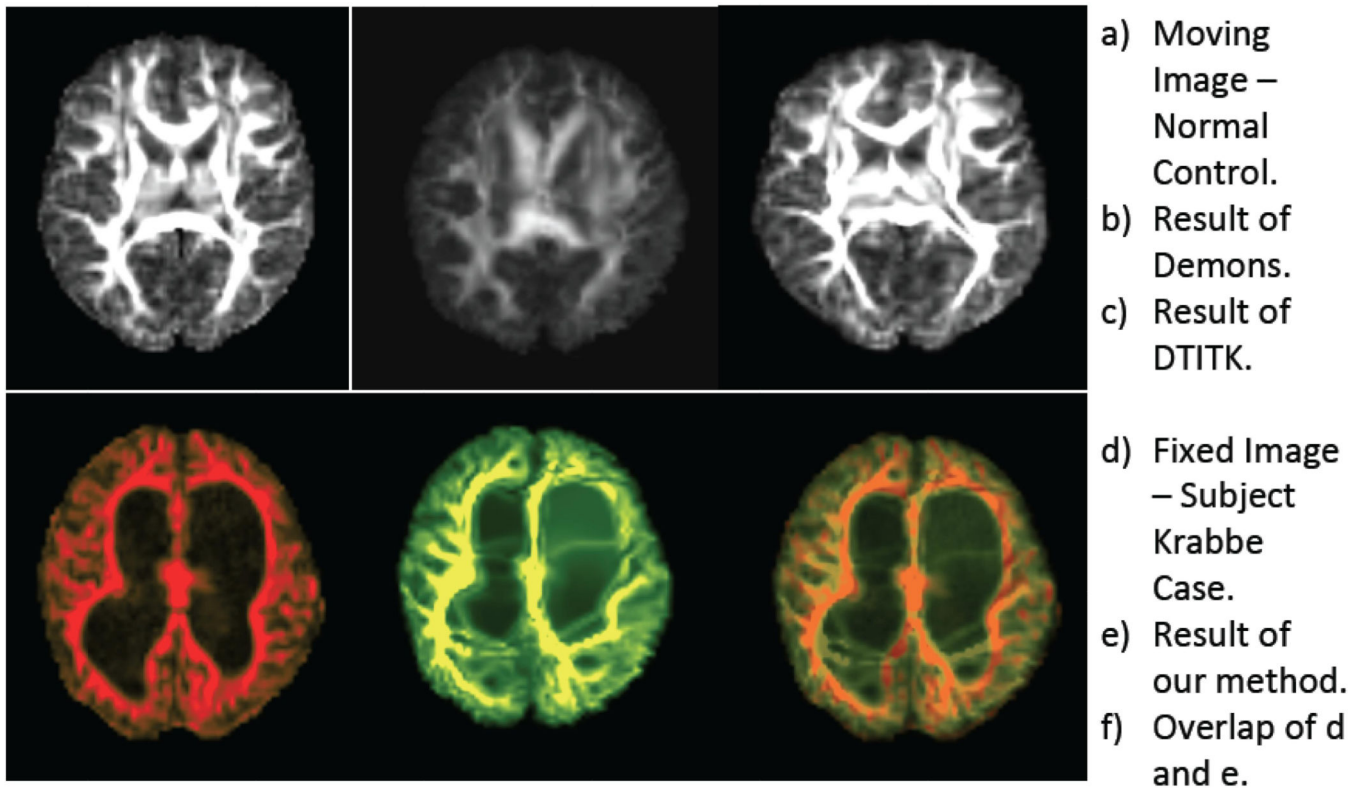
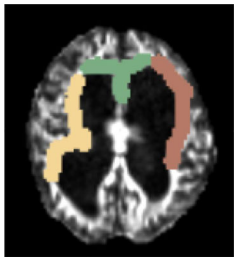


Figure 4.

The figure shows the normal control FA map, the Krabbe subject FA map with the registration result with demons, DTITK and our proposed method.



Label	Voxels Count	Demons	DTITK	Our Method
1	14288	48.057	49.344	73.351
2	13784	50.301	63.763	68.759
3	13448	46.020	53.519	70.784

Figure 5.
Labels on Krabbe case and percentage registration accuracy.